Precision Automatic Tracking Using a CW Laser

E. L. McGann
Applied Research Laboratory, Sylvania Electronic Systems

PRECISION AUTOMATIC TRACKING USING A CW LASER

by

E. L. McGann

APPLIED RESEARCH LABORATORY
Sylvania Electronic Systems
A Division of Sylvania Electric Products Inc.
40 Sylvan Road, Waltham, Massachusetts 02154

I. INTRODUCTION

This paper describes the design and performance of a precision CW laser tracker. When tracking low acceleration targets such as satellites and airplanes, this tracker has an accuracy of approximately 25 microradians rms. The accuracy under these conditions is set by the static friction, the background noise present in the equivalent noise bandwidth of the tracker and the scintillation of the atmosphere. When tracking high acceleration targets such as rockets, the tracker has a tracking error which is essentially proportional to the relative angular acceleration. If the rocket acceleration and the tracker-target geometry are such as to cause a relative angular acceleration of 0.6 radians/second^2, the tracking angular error peaks to 0.3 mr at the instant of launch settling to 0.1 mr within 0.1 second thereafter and remaining at the level during the rest of the propulsion period after which it reduces further to 25 microradians during the coasting phase.

Thus, the tracking accuracy against low acceleration targets is comparable to the accuracy of a star tracker. However, the laser tracker has the added capability of measuring range to the target. This accuracy particularly at low altitudes exceeds that which can be provided by a high performance radar.

Interest in high precision tracking, of course, results from the instrumentation tracking requirements that arise at the missile ranges and other test stations. High precision tracking is also a necessary part of long-range optical communications which can be efficiently accomplished only by using very narrow beams. The advantage of optical tracking over radar tracking is that it is not affected by undesired reflections from surrounding objects, and the accuracy is somewhat less affected by variations in the index of refraction of the atmosphere. Laser tracking, as contrasted to passive optical tracking, has the advantage of discriminating against other optical sources and also has the capability of simultaneously measuring range.

The system and the tests are described in Sections I and II respectively; system parameters are treated in the Appendix.

II. LASER TRACKING SYSTEM

A. General Description

The main components in this tracking system are a servo-controlled flat mirror, a large aperture parabolic mirror, an image dissector, and manual control facilities. The block diagram of this system is shown in Figure 1. The flat mirror on the servo mount, which is ten inches in diameter, is aimed to direct the transmitted signal at the target and to reflect the received signal onto an eight-inch diameter parabolic mirror. The parabolic mirror focuses the image to an image dissector which generates the error signals to drive the servo in the automatic mode. A periscope and manual-control console are included in this system for acquisition and manual tracking.

The laser source in this system is a 10-milliwatt He-Ne gas laser. The output of this laser passes through an optical modulator to the collimator and a series of mirrors and is finally incident on the servo-controlled flat mirror. The servo-controlled mirror and all other optical

elements are mounted on the main optical frame as shown in Figure 2. In order to conveniently transport the system from one site to another as the experimental test requirements dictate, this optical system is mounted in a van as shown in Figure 3.

Modulation is superimposed on the laser carrier to provide a range measurement capability. The relative phase between transmitted modulation and received modulation indicates the range to the target in a manner similar to the technique used in CW radars and altimeters. This tone modulation also serves the purpose of providing another means of discriminating against severe sky background gradients and other spurious signals. Also, if this tracker is used as one terminal for a communications link, intelligence can be impressed on the transmitted beam. The type of modulation can be selected such that this communication function need not interfere with the tracking function of the system.

The output of the modulator is focused by beam forming optics, and reflected off mirrors A and B (Figure 1) to the large servo-controlled tracking mirror. Mirrors A and B are also used in the initial alignment procedure to boresight the transmitted beam with the axis of the receiving optics. The transmitted laser beam reflected from the tracking mirror passes through the atmospheric path to the target. The energy intercepted by a retroreflective material on the target is returned to the tracking mirror along the original path direction.

The received signal is reflected off the tracking mirror and focused to a diffraction-limited point by the large parabolic mirror. The beamsplitter mirror C divides the signal so that part of the signal is fed through a 10Å filter to the range photomultiplier and the remainder is fed through a similar filter to an image dissector photomultiplier. The image dissector is an electronically scanned photomultiplier commonly used in star tracking applications as described by Atwill.[1] By removing the 10Å filter in front of the image dissector this tracker can track a noncoherent light source such as a star or satellite illuminated by the sun. This mode of operation is particularly useful in the initial acquisition stages in satellite tracking. With the 10Å filter replaced after initial acquisition the tracker can lock on the reflection of its own laser from a retroreflector on the satellite. Obviously, the tracker could also lock on a laser beacon carried by a remote target.

In actual operation, initial acquisition of the desired target is performed by an operator who looks through a wide angle boresighted periscope and manually positions the servo-controlled mirror. Upon seeing the return from the target, the operator switches from the manual mode to an automatic tracking mode.

B. Optics

The optical system is basically a Newtonian-type telescope with an 8-inch diameter, 96-inch focal length parabolic mirror used as the optical collector. The diffraction-limited spot for this mirror is 18 microns. The instantaneous field of view of the image dissector is 1 milliradian which extends about 2.5 mm in the focal plane, providing a better than 100:1 resolution of signal position. The image dissector scans in a rosette pattern over a 2 milliradian field of view as shown in Figure 4.

This image dissector tube generates the angular error signals for the tracking servo by examining the position of the target return signal in the image plane of the receiving optics. Each time the scan of the aperture passes through the image a pulse is formed in the output. When the image is centered within the scan this pulse train is symmetrical. When the image is displaced from the center of the scan as in Figure 4(b) an unsymmetrical pulse pair is generated from which azimuth and elevation signals are derived. The error sensing technique employed is again similar to that commonly used in star tracking systems employing image dissectors.

C. Servo Control System

The controlled member in the tracker is a two-axis gimballed mount on which is carried the flat directing mirror. Both axes of this mount are powered by DC torque motors directly coupled to the unit. Angular rate feedback information is obtained by DC tachometers which are also fastened directly to their respective axes.

The lowest structural resonance occurs about the azimuth axis at 45 c/s. This resonance limits the azimuth gain crossover frequency but does not significantly

affect the elevation loop. The rate loop gain crossover frequencies are 30 c/s in the azimuth and 50 c/s in the elevation channel. The position loop gain crossover frequencies are 10 c/s in azimuth and 17 c/s in elevation. Both axes have integral networks with an upper break frequency of 2 c/s and a lower break frequency at 0.02 c/s. The equivalent noise bandwidth for the tracker is 19 c/s in the azimuth and 30 c/s in the elevation.

High precision bearings of the ABEC class 7 type are used in both axes. Including the contributions from the various potentiometers, tachometers and motors, the measured static friction on both axes is 7×10^{-2} ft-lb. The static pointing accuracy on both axes is on the order of 10 microradians.

The dynamic performance which is quoted in connection with the rocket test data and also the low acceleration performance quoted in connection with the aircraft and satellite tracking tests are consistent with the system parameters given here.

III. TRACKING TESTS

The precision laser tracker has been used to track a retroreflector carried by a light airplane, a small rocket covered with Scotchlite retroreflective material, the Echo I satellite, and a + 7.5 visual magnitude star. Each of these tests reveals a particular characteristic of the tracker performance.

A. Rocket Tracking

Small rockets launched at an acceleration of about 13G were tracked when launched from a platform 670 feet from the tracker. These rockets are 1 foot long and 3/4 inch in diameter, and they are partially covered with a retroreflective cloth (also used for motion picture screens). Angular divergence of the reflected beam is about 5 microradians and the reflectivity is about 5 percent.

The 13G acceleration period lasts for approximately 2 seconds. The corresponding relative angular acceleration during the initial portion of this period is 0.6 radians/second^2. This acceleration results in a peak error of approximately 0.30 milliradian (see Figure 5). After the initial transient the error falls to approximately 0.1 milliradian while the rocket motor continues to burn. When the motor burns out the rocket is subject to drag and the deceleration of gravity, and the rocket is tracked during this coasting phase with an accuracy of 25 microradians rms.

Figure 6 shows one frame from a film recording of the rocket tracking tests. These films were taken through the operators telescope which is boresighted with the transmitting-receiving optics. The rocket appears at the telescope crosshairs. This particular frame shows the rocket as it is about to rise above the tree line. The environment for the test was chosen to be as challenging as possible. The launch area was placed down in a valley such that the tracker saw a background of vegetation. As the rocket rose the background viewed underwent extreme changes such as from trees to sky and finally the very bright sky background. The system consistently performed well under these adverse conditions.

B. Aircraft Tracking Tests

A retroreflector assembly bearing one retroreflector for each quadrant of the compass was mounted between the wheels of the light airplane. During the tests the aircraft would fly at different altitudes toward the tracking station starting from 10 to 15 miles away. The aircraft was visually spotted through the periscope and the laser beam, whose half power beamwidth was 0.7 milliradians, was pointed at the aircraft with the manual control system by the operator. Upon seeing the laser return from the retroreflector, the operator would switch the system into the automatic tracking mode.

Figure 7 shows a picture of the retroreflector-bearing aircraft taken during a tracking test run. The resultant error was less than $\pm$25 microradians rms. This error includes laser return signal angle of arrival fluctuations, and tracking errors due to relative angular rates which for this test ranged up to 2 degrees/second.

Aircraft tracking was successfully performed during the daylight at altitudes up to 10,000 feet (the maximum ceiling of the aircraft) at ranges of 9 to 15 km.

The system sensitivity was measured on a day when conditions approximated a Stand-

ard Clear Atmosphere[2]. The mid-afternoon southern horizon sky background intensity at an elevation of 5° was of the order of 0.4 $\frac{\text{watt}}{\text{ster-m}^2}$ in a 10Å bandwidth. The target was a 6.5-cm diameter precision retroreflector with an optical efficiency of 50 percent and a reflection divergence angle of 10 microradians. It was mounted on top of a 980-foot television tower approximately 11.0 km away. The measured signal level fluctuated by about a factor of two because of atmospheric turbulence effects. The peak signal power measured at the photocathode was 8×10^{-10} watts, and it produced a peak current signal to rms background induced shot noise in the image dissector's output 12 kc/s noise bandwidth of 20 to 1. This corresponds to 440 to 1 signal-to-noise ratio in the servo noise bandwidth of 25 c/s.

The unvignetted area of the collecting optics is 0.03 meters^2. The system optical efficiency, including the reflection loss off four reflecting surfaces, the narrowband filter transmission, and the signal beam splitter, is 0.2. Thus the power density at the input to the system was 1.3×10^{-7} watts/m^2. The system equivalent noise background power input as determined from the signal-to-noise ratio is 3×10^{-10} watts/m^2 referred to the servo bandwidth of 25 c/s. Assuming that the system optical efficiency was 20 percent and that the atmospheric transmission was 0.06 based upon a 24-km visibility measurement of the Boston Weather Bureau and an average path altitude of 0.5 km^2 with an average attenuation coefficient of 0.12/km^2 and that the retroreflector efficiency was 50 percent, the calculated expected signal power P_s is $P_s = 2.7 \times 10^{-9}$ watts. The measured signal power return was 7×10^{-10} watts, a discrepancy of about a factor of three. The most probable sources of this discrepancy are in our estimate of the atmospheric transmission and the possibility that there might be some dirt accumulation on the retroreflector mounted on the television tower.

To maintain a tracking accuracy of 25 microradians requires a signal-to-noise ratio in the servo bandwidth of about 40:1[3,4]. If the tracking experiments had been conducted under the visibility conditions present during the sensitivity measurement we might reasonably expect to track to a range of 16 km at these low elevation angles. Since the atmospheric absorption effect enters the signal power calculation as an exponential function, the signal-to-noise ratio decreases very rapidly at long ranges and low altitudes. Hence the successful tracking over ranges of 9 to 15 km is satisfactory.

C. Satellite Tracking

The precision tracker has locked on and tracked the Echo satellites using the reflection of the sun for the input signal. Plans are being made to track the S-66 satellite actively with this CW laser system using the passive tracking mode only during the initial acquisition phase. Satellites are acquired using trajectory data computed by the Smithsonian Astrophysical Laboratory. This data gives the azimuth and elevation of the satellite at minute intervals throughout its path. To acquire the satellite the field of view of the tracker is pointed at the computed azimuth and elevation coordinates; the system then waits for the satellite to pass through the field of view. When the satellite appears in the field of view the tracker is manually operated to bring the satellite onto the cross hairs at which time it is switched to automatic tracking.

Figure 8 is a photograph of the Echo I satellite during a 10 minute tracking run. During this run the tracking error was approximately 17 microradians rms. The angular velocity of the satellite is roughly 0.5° per second. The Echo I satellite is a comparatively bright source for tracking, being equivalent to a +1.0 magnitude star.

Furthermore, these nighttime tests are an ideal opportunity to check the ultimate sensitivity of the system.

From signal-to-noise measurements on the bright star Vega it has been determined that the threshold signal that this system can detect is 3×10^{-14} watts/meter^2. This magnitude signal will yield a unity signal-to-noise ratio on the 25 c/s servo bandwidth. This is comparable to +12.5 magnitude star. The system has actually locked on a 7.5 magnitude star, but we are temporarily prevented from going to fainter stars by the effect of sky glow on the acquisition technique. Changes presently underway on the opera-

tor's telescope characteristics and the system field of view will allow lesser stars to be acquired.

APPENDIX

SYSTEM PARAMETERS

A. Range Parameters

Consider the system transmits a signal power P_T in a solid angle Ω_T. Then the amount of power, assuming a lossless transmission path, intercepted by a retroreflector on the target being tracked is

$$\frac{P_T \Omega_R}{\Omega_T} \tag{1}$$

where Ω_R is the solid angle subtended by the retroreflector. Normally with a perfect retroreflector the reflected power diverges at an angle Ω_R. However, if the retroreflector departs from a perfect right trihedral angle by Ω_e then an additional divergence is added to the reflected beam. Then the power reflected from the retroreflector diverges at an angle $\Omega_R + \Omega_e$.

If the receiver optics subtend the angle $\Omega_R + \Omega_e$ all the energy is collected by the receiver. If it is assumed that the optics subtend a smaller angle of the source radiation Ω_o, then the power collected by the receiver is

$$\frac{P_T \Omega_R \Omega_o}{\Omega_T \left(\Omega_R + \Omega_e \right)} . \tag{2}$$

In addition, if an atmospheric transmission T and an overall optical efficiency E is assumed then the signal power P_s received by the tracking image dissector is given by Equation (3) as

$$P_s = \frac{ET\, P_T \Omega_R \Omega_o}{\Omega_T \left(\Omega_R + \Omega_e \right)} \tag{3}$$

where the optical efficiency E includes system reflection, scattering, filter and beamsplitter losses.

When the system is operating at distance R between the tracker and the target the solid angles Ω_R and Ω_o are given by Equations (4) and (5):

$$\Omega_R = \frac{A_R}{R^2} \tag{4}$$

$$\Omega_o = \frac{A_o}{4R^2} \tag{5}$$

where A_R is area of the retroreflector and A_o is the effective collecting aperture of the optics. Substituting Equations (4) and (5) in Equation (3) yields the expression for the received signal power:

$$P_s = \frac{ET\, P_T A_R A_o}{4\Omega_T R^2 \left(A_R + R^2 \Omega_e \right)} \tag{6}$$

B. Signal-to-Noise Ratio

In the image dissector photodetector the photocathode signal current i_s is given by the expression

$$i_s = \rho P_s \tag{7}$$

where ρ is the photocathode responsivity and P_s is the signal power of Equation (6).

Assuming a uniform radiation background the rms shot noise current $\bar{I}_n$ is

$$\bar{i}_n = \sqrt{2e\Delta f \left[I_b + \rho P_s + \rho P_B \right]} \tag{8}$$

where

- e is the electronic charge
- Δf is the system noise bandwidth
- I_D is the thermionic dark current
- P_B is the background power passing through the 10Å optical filter.

The ultimate signal-to-noise power ratio S/N of the overall system with a bandwidth of Δf can be shown to be[5]

$$\frac{S}{N} = \frac{\rho^2 P_s^2}{2e\Delta f \left(I_D + \rho P_s + \rho P_B \right)} \tag{9}$$

C. Errors in Closed Loop Tracking Systems

The primary consideration in determining the setting of the tracking loop gain-crossover frequency (loop bandwidth) is to ensure that the servo system will have sufficient dynamic response capability so as to be able to follow the target with the desired accuracy while undergoing the relative angular rates imposed by the tracker-target geometry.

Assuming that the relative motion of the target during the tracking interval has frequency components low in comparison to the tracking loop gain-crossover frequency, References 6 and 7 show that the angular errors can be quite accurately expressed as

$$\theta_e(t) = \frac{\dot{\theta}_i\left(t - 1/\omega_i\right)}{\beta\omega_c} + \frac{\ddot{\theta}_i\left(t - 1/\omega_i\right)}{\omega_c\omega_i} \qquad (10)$$

where

ω_c = gain crossover frequency of the position feedback loop of the tracking system

ω_i = upper break frequency of the integral network in the position feedback loop

β = ratio of break frequencies of the integral network.

This equation states that the error is due in part to the input velocity $\dot{\theta}_i$ at time $\left(t-1/\omega_i\right)$ and in part to the input acceleration $\ddot{\theta}_i$ at the time $\left(t-1/\omega_i\right)$.

Very often the tracking error is expressed as an error-coefficient expansion which theoretically employs an infinite series derivation of the input. Equation (10) is equivalent to the error-coefficient expansion with the effect of the higher order derivatives included within the $\left(1/\omega_i\right)$ time delay of the acceleration term.

On the other hand, the ultimate system performance is a function of the signal-to-noise ratio in the system and since the closed-loop tracking system acts as the noise filter the performance of the system in terms of the S/N ratio derived in the previous section can now be determined.

Using methods similar to those employed by Develet[3,4], the rms error in a closed-loop tracking system can be given by

$$\theta^2_{rms} = K^2\,\frac{\Phi\Delta f}{S} = K^2\left(\frac{N}{S}\right) \qquad (11)$$

where again

S = signal power

Δf = system noise bandwidth

and

Φ = low frequency noise-power spectral density

K = slope of the reciprocal of the error curve in units of θ.

It remains now only to determine Δf for the particular closed-loop configuration used so that the rms system error as given in Equation (11) will be completely specified. The noise bandwidth is defined as

$$\Delta f = \int_0^\infty \left|G(f)\right|^2 df \qquad (12)$$

where G(f) equals the closed loop transfer function of the tracking system. For a tracking system whose gain-crossover frequency is f_c and which has an integral network in the position feedback loop whose upper break frequency is f_i, the noise bandwidth of the closed loop tracking system is

$$\Delta f = \frac{\pi}{2}\left(f_c + f_i\right) . \qquad (13)$$

The noise bandwidth of this tracking system is 25 c/s. Thus the rms tracking error of a simple closed loop system can be given in terms of the system S/N ratio, error curve, and control loop parameters as

$$\theta^2_{rms} = \frac{\pi K^2_e}{\rho^2 P^2_s}\left(f_c + f_i\right)\left(I_o + \rho P_s + \rho P_B\right) . \qquad (14)$$

D. Radiation Background Discrimination[8,9]

In any optical detection, tracking, or communication system, background noise can

limit the system range. During the daytime, solar radiation either direct or specularly reflected from objects is a source of very intense radiation. Less intense but still quite significant is the solar radiation scattered from clouds, haze, air or earthbound objects. At night the stars, skyglow and solar reflections from satellites, the moon, and other planets all constitute the background. If the background present in the field of view of the image dissector is uniform then the net result is the production of a random shot noise component in the photocurrent proportional to the square root of the background power. If gradients are present in the background or in any way are introduced by the optical system then these gradients are detected by the scanning action of the image dissector and produce signals directly proportional to the background gradients being scanned. The range photomultiplier is not affected by gradients because no scanning is performed. However, if the background field is moving because the system is tracking a fixed target, the change in background level is directly detected.

The laser optical tracker uses two means to discriminate against background. One involves modulating the laser signal while the second utilizes optical filtering at the laser frequency. The use of a modulation on the transmitted beam provides a technique allowing the system to discriminate against gradients and changes in level by means of electrical filtering. A bandpass electrical filter at that modulation frequency is used following the image dissector output. The modulation frequency is chosen to exclude signal components produced by background gradient scanning and level changes. This technique has been implemented in the laboratory but has not yet been installed in this optical tracking system.

For our preliminary testing we have found that a 10Å wide optical interference filter reduced most background to an operable value for the tests performed. As the system range is extended the modulation technique will be necessary to discriminate against cloud edges and the horizon in the daytime. Narrower interference filters will also be required to reduce the uniform level further.

E. Atmospheric Transmission and Refraction[10]

The wavelength of operation of the system is 6328Å. At this wavelength there are no predominant absorption bands in the atmosphere.[11] The principal loss of signal is due to scattering. Both Rayleigh and aerosol scattering are significant especially over long slant range paths.

Even for a Standard Clear Atmosphere the exponential attenuation coefficient due to scattering would be 0.17/kilometer for a horizontal path.[2] Thus, for a long nearly horizontal path, this loss is significant. However, when tracking near the zenith it is negligible. As the visibility is limited by increased haze conditions and of course clouds, the tracking system would be similarly limited.

Variations in index of refraction along the beam path will divert the beam. However, if the time variations of the index are small compared to the beam transit time then the outgoing beam axis is the same as the return beam. Because the index of refraction does vary with temperature, pressure, and water vapor contents, the angular direction of the target as measured from the mirror position angles is only an apparent direction.

Atmospheric turbulence[12,13] produced primarily by the thermal gradients can limit this type of system. The turbulent air consists of time varying parcels of different indices of refraction. The atmospheric shimmer observed over near ground paths and at exact apertures such as windows is typical of this phenomenon. Time varying refractions over the transmission path produce transmitter beam line-of-sight variations that make it difficult to point very narrow laser beams and thus limits usable beamwidths. Also angle of arrival variations at the receiver aperture limit the system resolution.

The system described herein is the result of a joint effort by the members of the Electro-Optic group of the Sylvania Applied Research Laboratory including Dr. C.J. Peters, R.L. Lucy, K.T. Lang, and G. Ratcliffe.

REFERENCES

1. U.D. Atwill, "Star Tracker Uses Electronic Scanning," Electronics, McGraw-Hill, 30 September 1960.

2. L. Elterman, "Parameters for Attenuation in Atmospheric Windows for Fifteen Wavelengths," Applied Optics, vol. 3, no. 6, p. 745; May 1964.

3. J.A. Develet, "Thermal Noise Errors in Simultaneous-Lobing and Conical Scan Angle-Tracking Systems," IRE Transactions on Space Electronics and Telemetry, pp. 42-51; June 1951.

4. E.K. Sanderman, "Criterion for Angular Noise in Star-Lock Systems," IRE Transactions on Aerospace and Navigational Electronics, pp. 21-23; March 1962.

5. G. Biernson and R.F. Lucy, "Requirements of a Coherent Laser Pulse Doppler Radar," Proceedings of the IEEE, vol. 51, no. 1; January 1963.

6. G. Biernson, "A Simple Method for Calculating the Time Response of a System to an Arbitrary Input," AIEE Transactions, Applications and Industry, pp. 227-247; September 1955.

7. G. Biernson, "Estimating Transient Response from Open Loop Frequency Response," AIEE Transactions, Applications and Industry, pp. 388-403; January 1956.

8. J.I. Gordon, "Optical Properties of Objects and Backgrounds," Applied Optics, vol. 3, no. 5, p. 556; May 1964.

9. L.M. Biberman, "Background Consideration in Infrared System Design," Applied Optics, vol. 4, no. 3, p. 343; March 1965.

10. A.R. Boileau, "Atmospheric Properties," Applied Optics, vol. 3, no. 5, p. 570; May 1964.

11. J.A. Curcio, L.F. Drunmeter, and G.L. Knestrick, "An Atlas of the Absorption Spectrum of the Lower Atmosphere from 5400Å to 8520Å," Applied Optics, vol. 3, no. 12, p. 1401; December 1964.

12. B.N. Edwards, and R.P. Steen, "Effects of Atmospheric Turbulence on the Transmission of Visible and Near Infrared Radiation," Applied Optics, vol. 4, no. 3, p. 311; March 1965.

13. D.J. Portman, et al, "Some Optical Properties of Turbulence in Stratified Flow Near the Ground," Journal of Geophysical Research, vol. 67, no. 8, p. 3223, July 1962.

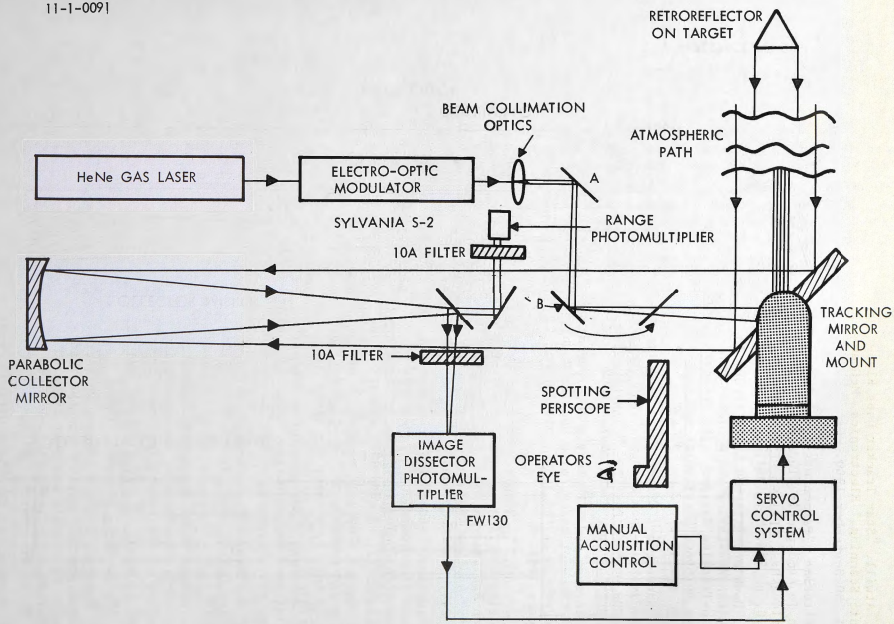

Figure 1. Precision CW Laser Tracking System.

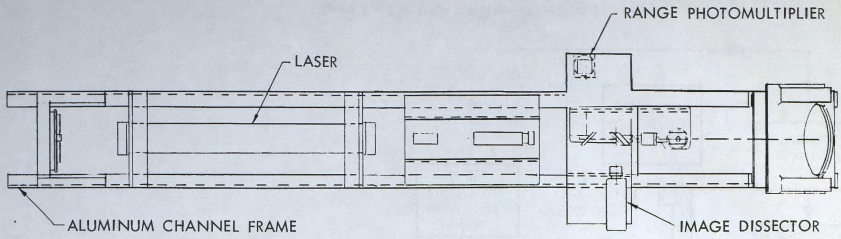

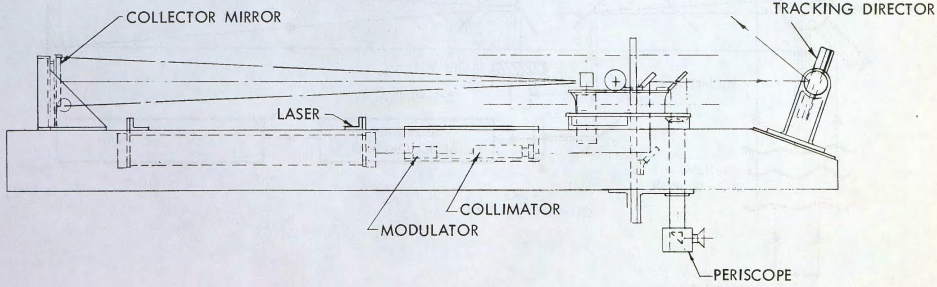

Figure 2. Optical Layout.

Figure 3. Laser Tracking System Van.

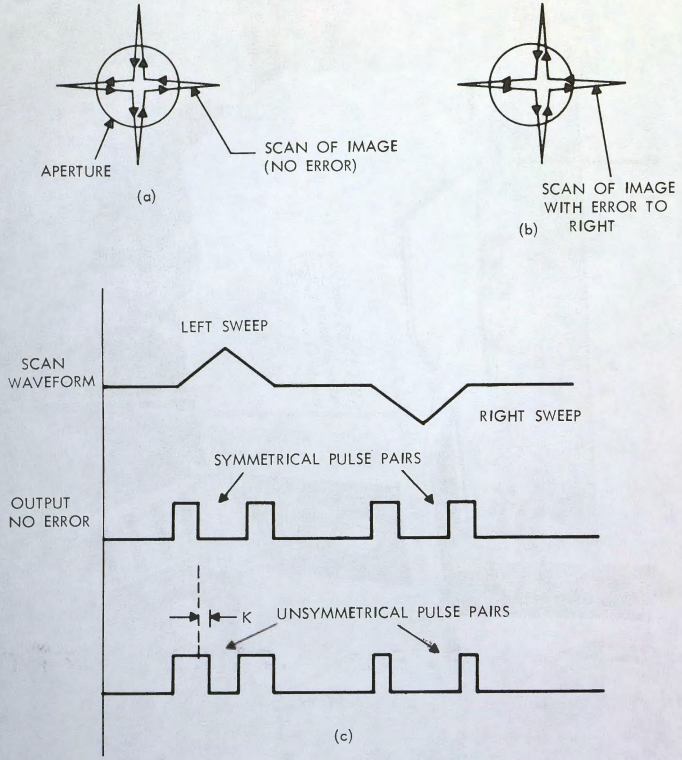

Figure 4. Image Dissector Sweep and Output Waveforms for One Axis with and without Position Error.

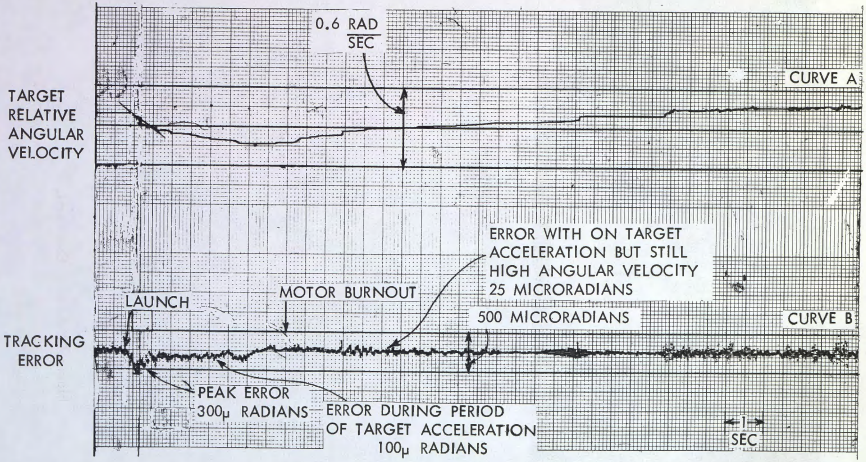

Figure 5. Error Data During Rocket Tracking Tests.

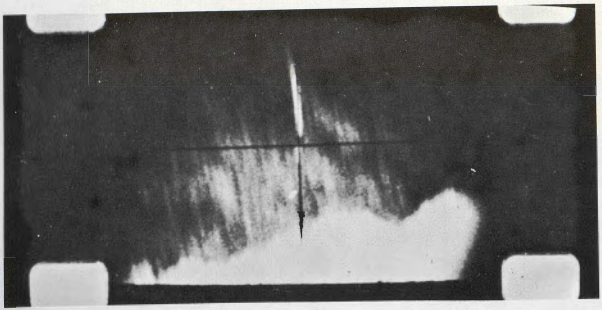

Figure 6. Rocket Track During Launch.

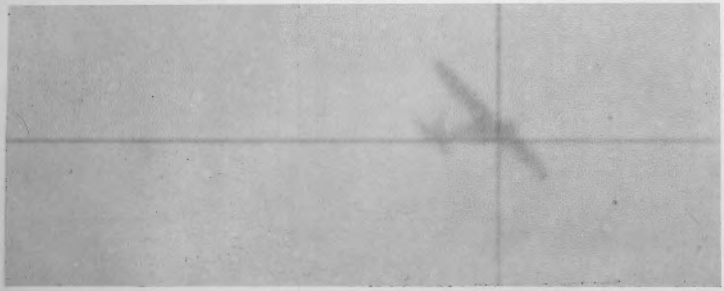

Figure 7. Aircraft Overhead.

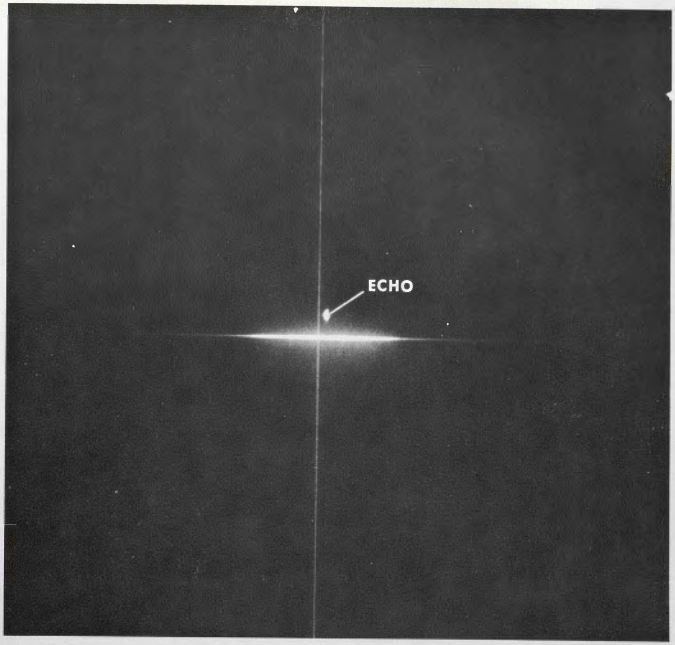

Figure 8. Echo I.